Appeared in Proceedings of Computer Vision and Pattern Recognition Workshop on Biometrics (CVPRW), (New York, USA), June 2006

Multispectral Iris Analysis: A Preliminary Study

Christopher Boyce, Arun Ross, Matthew Monaco, Lawrence Hornak and Xin Li

Lane Department of Computer Science and Electrical Engineering
West Virginia University, Morgantown, WV 26506 USA
cboyce@mix.wvu.edu, arun.ross@mail.wvu.edu, mmonaco@mix.wvu.edu,
lawrence.hornak@mail.wvu.edu, xin.li@mail.wvu.edu

Abstract

This paper explores the possibility of using multispectral iris information to enhance the recognition performance of an iris biometric system. Commercial iris recognition systems typically sense the iridal reflection pertaining to the near-infrared (IR) range of the electromagnetic spectrum. This work examines the iris information represented in the visible and IR portion of the spectrum. It is hypothesized that, based on the color of the eye, different components of the iris are highlighted at multiple wavelengths. To this end, an acquisition procedure for obtaining co-registered multispectral iris images associated with the IR, Red, Green and Blue wavelengths of the electromagnetic spectrum, is first discussed. The components of the iris that are revealed in multiple spectral channels/wavelengths based on the color of the eye are studied. An adaptive histogram equalization scheme is invoked to enhance the iris structure. The performance of iris recognition across multiple wavelengths is next evaluated. Experiments indicate the potential of using multispectral information to enhance the performance of iris recognition systems.

1. Introduction

Commercial iris recognition systems operate predominately in the *near-Infrared* (IR) range of the electromagnetic spectrum. The intricate textural pattern represented in different colored irides is revealed in the near-IR range and has been traditionally used as a biometric indicator [1]. In this work, we explore the possibility of eliciting iridal information from the *visible* and IR ranges of the reflected light. In particular, we study the role of information represented in individual spectral channels/wavelengths (i.e., IR, Red, Green, and Blue) on iris recognition and explore the feasibility of decomposing the structural components of an iris based on the response of individual channels. To the best of our knowledge, this is the first attempt to study the multispectral response of the iris tissue from a biometric perspective.

This paper describes the following: (a) multispectral image acquisition; (b) iris image segmentation; (c) visual analysis of iris structure as revealed by individual spectral channels; (d) adaptive histogram equalization using color information; (e) evaluating matching performance across different channels/wavelengths; (f) clustering iris-pixels in RGB space in order to decompose multiple components of the iris; and (g) examining the possibility of fusing information contained in multiple channels. The primary goal of this paper is to initiate systematic research in multispectral iris analysis.

2. Structure and Pigmentation of the Iris

To better appreciate the significance of multispectral iris analysis, we present a brief overview of the textural intricacies of the iris anatomy. The purpose of this section is to emphasize individual iris components that may exhibit different reflectance characteristics thereby justifying a multispectral analysis.

2.1. Iris anatomy

A cross section of the iris reveals two layers: the anterior stroma layer and the posterior epithelial layer.

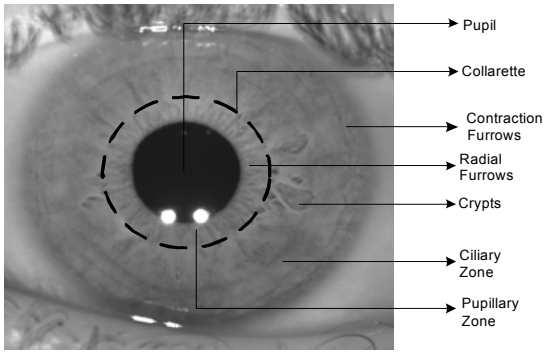

Figure 1. Anatomy of the anterior portion of the iris.

The *anterior* portion of the iris is the foremost visible portion of the eye (Figure 1). Therefore, it is easily imaged and is the focus of all iris recognition systems. The anterior surface of the iris is separated into two zones: the pupillary zone and the ciliary zone. These two zones are divided by a circular zigzag ridgeline known as the collarette. The two zones on the surface of the iris often differ in color. Many pit like oval structures appear mainly in the zone around the collarette and the outer edge of the iris. These structures are called crypts (Fruch's crypts) and they permit fluids to quickly enter and exit the iris during dilation and contraction of the pupil.

The anterior surface has a velvety appearance showing a series of radial streaks that are caused by trabeculae or bands of connective tissue that enclose the crypts. These radial streaks straighten when the pupil is constricted and

turn wavy when the pupil is dilated. Near the outer part of the ciliary zone concentric lines can be seen. These lines become deeper as the pupil dilates and are called contraction furrows. These lines, caused by the folding of the iris as the pupil dilates, are easily seen in darkly pigmented irides. At the pupillary margin, the heavily pigmented epithelium extends around the edge of the pupil. The radial folds of the epithelium give the pupillary margin a sort of beaded or pearl appearance. This region is termed the pupillary fringe or ruff. The average diameter of the iris is approximately 12mm, with an average thickness of about .5 mm, thickest at the collarette and thinning radially away from the pupil.

The posterior layer of the iris is composed of two pigmented epithelial layers. The anterior layer lies in contact with the stroma and is associated with the muscular process of the dilator pupillae. This layer contains relatively few melanin granules. The posterior layer cells are larger than the anterior layer and cubical in shape. They are stacked together in a compact and orderly arrangement and are heavily composed of melanin granules.

The iris's main function is to regulate the amount of light that can enter the eye and impinge on the retina. It does this through dilation and constriction of the pupil. In low light conditions the dilator pupillae muscle is triggered through parasympathetic nerve activity and dilates the iris to allow in more light. In bright or intensive light conditions the constrictor pupillae muscle is triggered through parasympathetic and sympathetic nerve activity that dilates and constricts the pupil.

2.2. Iris Pigmentation

The iris can vary in color from light blue to dark brown [9]. This variation can be (a) across the population, (b) between the left and right eyes of an individual, or (c) in different regions of the iris in the same eye. The main contributors of color are the cellular density in the extracellular matrix of the iris stroma (vascular connective tissue containing collagen fibers, fibroblasts, melanocytes, nerve fiber, smooth muscle, myoepithelial cells, radial vessels, and matrix), the pigment contained in the iris stroma and the pigment contained in the iris pigment epithelium (IPE) layer. Studies indicate that the amount and distribution of melanin in the IPE is similar in irides of different color. Therefore, it is less representative of the iris color than the stroma. So, the color of the iris relies on the cellular density of the stroma and more heavily on the pigmentation of the stroma. Heavy melanin synthesis corresponds to a dark brown iris, whereas light melanin synthesis corresponds to a light blue iris. Impinging light on the iris gives the appearance of color. Longer wavelength light readily penetrates the iris and is absorbed. However, shorter wavelength light (blue light) is reflected back and scattered by the iris stroma. Thus, irides with low pigmentation have a bluish appearance.

2.3. Multispectral Imaging

A multispectral image contains information across multiple wavelengths (or wavelength bands) of the electromagnetic spectrum. Multispectral imaging has been used in diverse fields such as geospatial and medical imagery, as well as in biometric analysis (e.g., face [4][5][6], finger [7]). Through the use of multispectral imagery, an iris can be broken down into its own unique reflection pattern according to its phenotypical traits.

3. Iris Image Acquisition

To capture the different wavelengths being reflected from an iris, the following arrangement using Redlake's MS3100 multispectral camera was employed. The camera incorporates three charge coupled devices (CCD) and three band-pass prisms behind the lens to simultaneously capture four different wavelength bands (Figure 2).

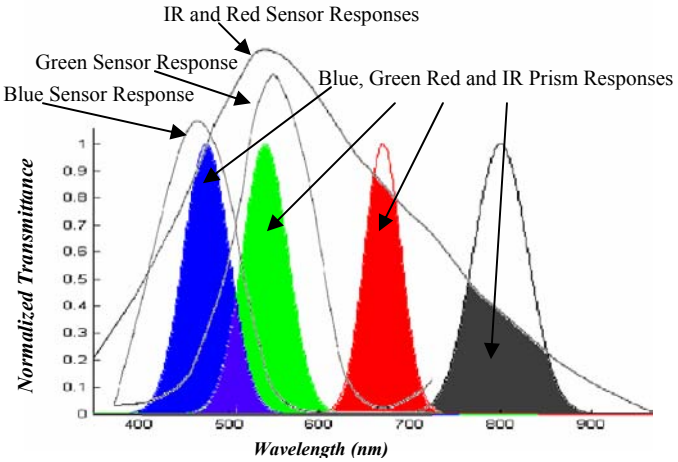

Figure 2. The normalized transmittance of the band-pass prisms and sensor spectral response of the acquisition device. Filled portions of the graph indicate the actual combined response of the sensors and prisms.

The IR and Red (R) sensors of the multispectral camera are two separate Sony ICX205AL sensors whose spectral response ranges from 400nm to 1000nm with a peak response at 550nm. The Green (G) and the Blue (B) channels are recorded on the same Sony RGBICX205 sensor. This sensor is a RGB sensor with a blue response from 400nm to 550nm (peaking at 460nm) and a green response from 400nm to 650nm (peaking at 550nm). Each channel is white-balanced (manually) to ensure a maximum intensity of 255 by using the white panel of a color checker chart. It must be pointed out that the

resolutions of the images in the multiple spectral channels are not all the same. The IR and Red sensor output an image of size 1300x1040. This represents an average of 56,000 pixels inside the segmented iris. The G and the B images are recorded on a RGB Bayer pattern sensor and are, therefore, one-third the resolution of the other images. The G and the B images are extracted and scaled to have the same resolution as the IR and R images using linear interpolation of the nearest neighbors [8]. The primary advantage of using a camera that has three CCD sensors/prisms and a single lens is that the resulting images are all spatially registered. Therefore, no explicit image registration or alignment across multiple channels is necessary when processing the images.

This arrangement acquires spectral information as follows: (a) red light at a center wavelength of 670nm and a band pass of 40nm, (b) green with a center wavelength of 540nm and a band pass of 50nm, (c) blue with a center wavelength of 475nm and a band pass of 50nm, and (d) near-IR with a center wavelength of 800nm and a band pass of 60nm as shown in Figure 2.

To image the iris accurately and in a convenient fashion, the multispectral camera was mounted onto an ophthalmologist's slit-lamp mount (Figure 3). The mount consisted of a chin rest, to position the head, and a mobile camera-mount arm that could be easily manipulated to finely focus on the iris.

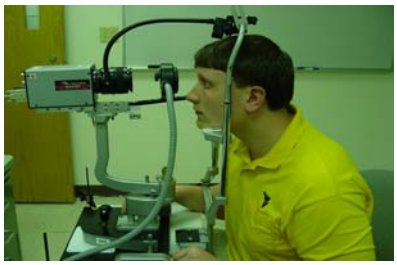

Figure 3. The multispectral iris image acquisition arrangement.

A broadband light source was employed to illuminate the iris of the eye. The spectral output of the light source ranged from 350nm to 1700nm. The illumination was projected on the eye using a fiber optic light-guide with a ring light attached at the illumination end. This projects a circular uniform illumination across the eye. However, it does produce a large ring reflection on the moist cornea of the eye, as opposed to a small point source reflection from LEDs commonly seen in most iris imaging systems.

4. Multispectral Data Analysis

The optical arrangement described in the previous section was used to acquire data from 24 subjects (5 samples per subject). The subject pool used in this preliminary analysis consisted of individuals having different eye colors as recorded in Table 1. The color of each iris was determined by visual inspection since it is difficult to automatically elicit the eye color from the images given the rapid variations in texture chromaticity within the high-resolution image. Figure 4, Figure 5 and Figure 6 show the intensity of iridal reflection across the four channels for different eye colors. Note that the CIR (color infrared) images are obtained by dropping the blue channel and including the IR channel (these are false color images). The graphical plots in these figures indicate the variation in pixel intensity across the four channels as one moves radially outward from the boundary of the pupil/iris toward the boundary of the iris/sclera.

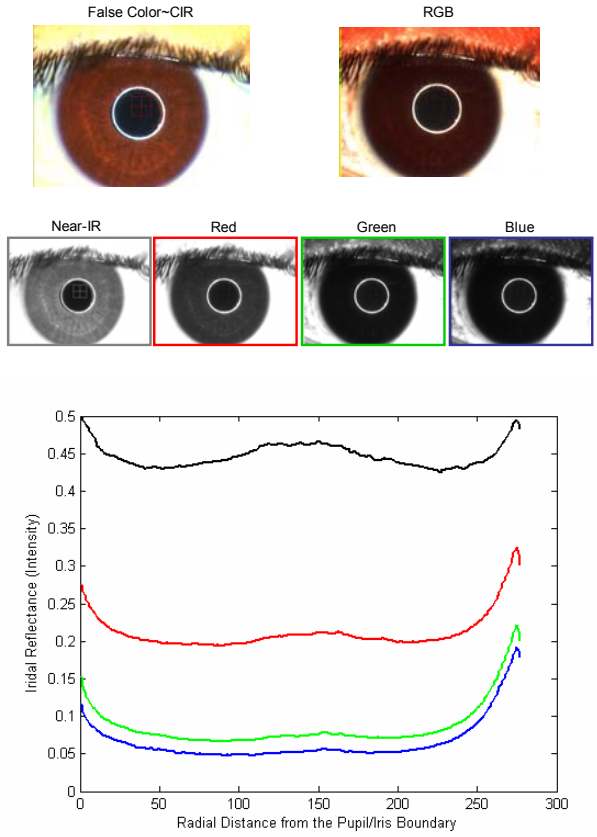

Figure 4. Example of a dark brown iris. The iris exhibits high iridal reflectance in the IR channel. The reflectance is observed to decrease significantly with wavelength.

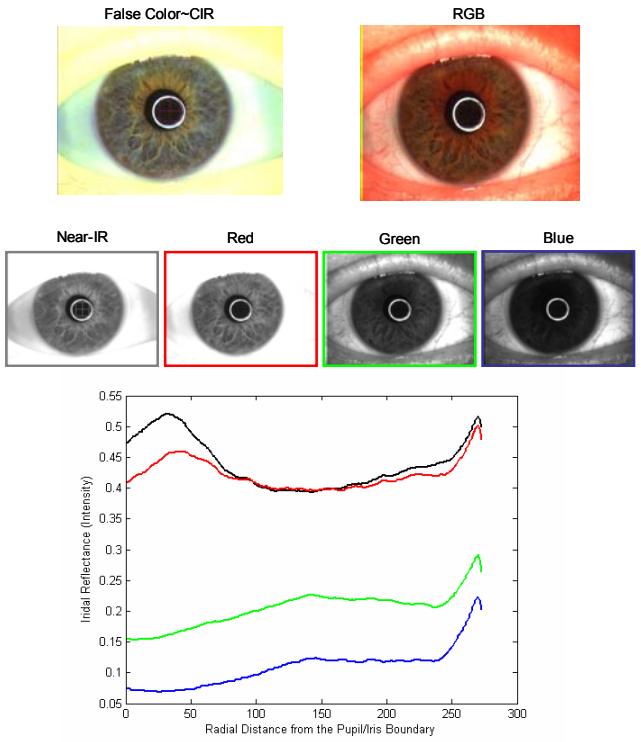

Figure 5. Example of a light-brown/green iris. The iris exhibits high iridal reflectance in the IR and Red channels. Reflectance decreases significantly with other wavelengths.

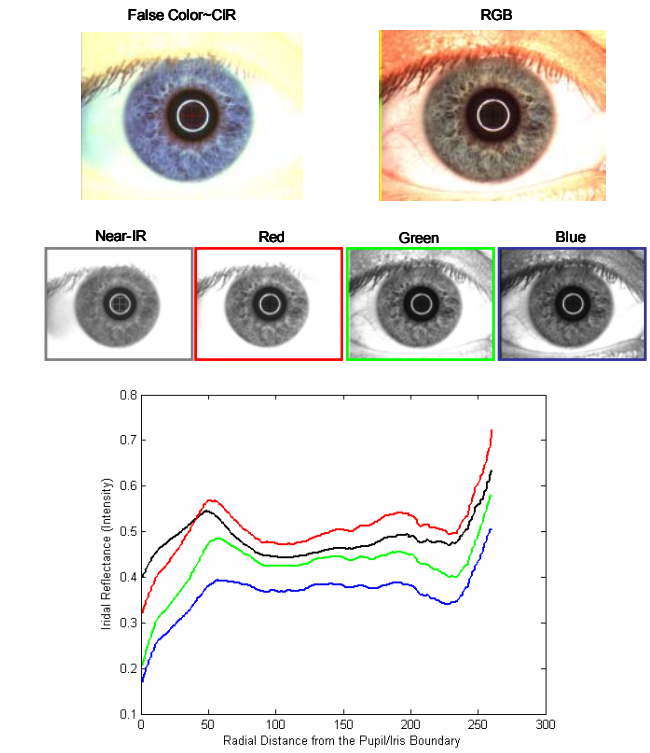

Figure 6. Example of a blue iris. The iridal reflection is comparable across all four channels.

TABLE 1. VISUAL ASSESSMENT OF EYE COLOR FOR THE 24 SUBJECTS. NOTE THAT BROWN IRIDES EXHIBIT VARIATIONS RANGING FROM DARK-BROWN TO LIGHT-BROWN. THE REFECTANCE PROPERTY OF SUCH IRIDES VARIES WITH THE 'SHADE' OF BROWN OBSERVED.

	RGB Color
User 1	Brown (Dark)
User 2	Brown (Dark)
User 3	Brown (Dark)
User 4	Brown (Light)/Green(Hazel)
User 5	Brown (Dark)/Brown(Yellow)
User 6	Brown (Light)/Brown(Gray)
User 7	Brown (Dark)
User 8	Brown (Light)/Brown(Yellow)
User 9	Gray(Blue)/Blue
User 10	Gray(Blue)/Blue
User 11	Brown (Yellow)/Gray(Blue)
User 12	Brown (Light)/Green(Hazel)
User 13	Gray
User 14	Brown (Dark)/Brown(Light)
User 15	Brown (Light)
User 16	Brown (Dark)
User 17	Blue(Gray)
User 18	Brown(Dark)/Brown(Light)
User 19	Brown(Dark)/Brown(Light)
User 20	Brown/Gray(Yellow)
User 21	Brown
User 22	Brown(Light)/Blue(Yellow)
User 23	Brown
User 24	Brown (Dark)

5. Segmentation

Segmentation involves the automatic localization of the spatial extent of the iris structure by detecting its boundary in the image and designing a mask of '1's and '0's indicating the iris and non-iris regions, respectively ([1][2][3]). It is a crucial first step in any iris processing algorithm. The approach used in this paper can be divided into two stages: the pupillary boundary detection (between the pupil and iris) and the limbic boundary detection (between the iris and the sclera). A simple scheme was implemented, since the primary focus of this paper was on image analysis. Note that in the current implementation, the segmentation algorithm is applied independently to the individual channels (Figure 8).

1. Pupillary boundary detection: A combination of simple binary thresholding and morphological closing was used to detect the pupil and eliminate the ring-light reflection. The reflection of the ring-light, in many instances, was constrained almost entirely to the pupil thereby necessitating the application of a closing operator after binary thresholding. Due to the propensity of this algorithm to detect eyelashes as well as the pupil, a 'connectivity' test was conducted to distinguish between these two entities. The pupil, in general, was observed to occupy a larger area than the eye lashes. Upon detecting the pupil (as the largest vertically connected object), its boundary was tracked on a pixel-by-pixel basis.

2. Limbic boundary detection: The location of the pupillary boundary was used as a starting 'point' to initiate the search for the limbic boundary. A set of rectangular regions-of-interest (ROIs) were first selected in the vicinity of this boundary and the horizontal intensity gradient information in each region was computed. A prominent peak in the computed information indicated the possible presence of the limbic boundary. The location of the peak was used to define a circular region-of-interest about the center of the pupil. The area within this circular ROI was subjected to a dynamic thresholding scheme in order to isolate the iris information. The proposed scheme may not be efficient in those channels where there is lack of contrast between the eyelashes, eyelids and iris.

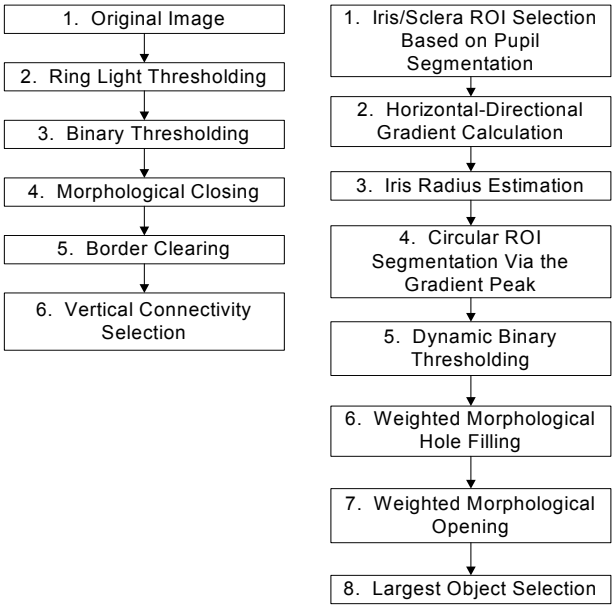

Figure 7(a). Pupillary (left panel) and Limbic (right panel) boundary segmentation algorithm.

The resulting segmentation isolates the entire iris from the pupil, the sclera, upper and lower eyelids, and the eyelash boundary. The result of segmentation on each of the individual channels can be seen in Figure 8. One of the advantages of using multispectral information is the possibility of conducting segmentation in multiple spectral channels and *fusing* the result to obtain a single global segmentation. Specifically, the presence of eye lashes and eye lids may be more easily detected in certain spectral channels than others.

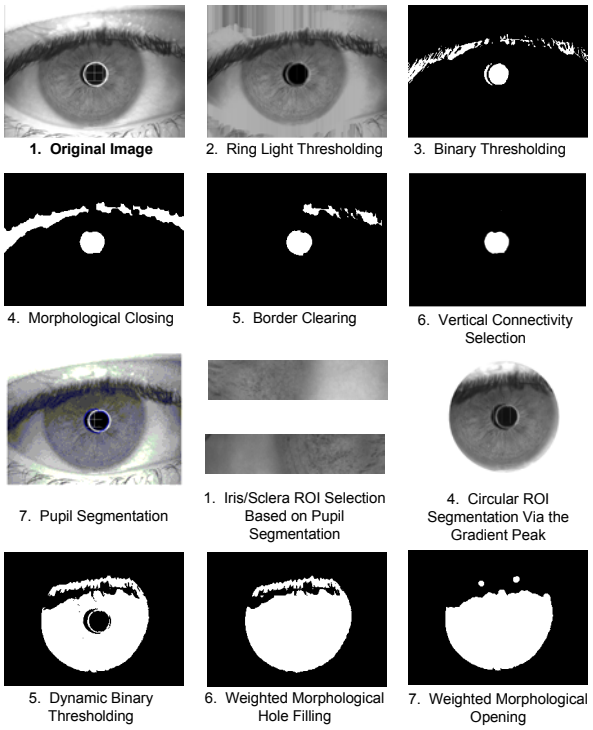

Figure 7(b). Illustration of the segmentation procedure.

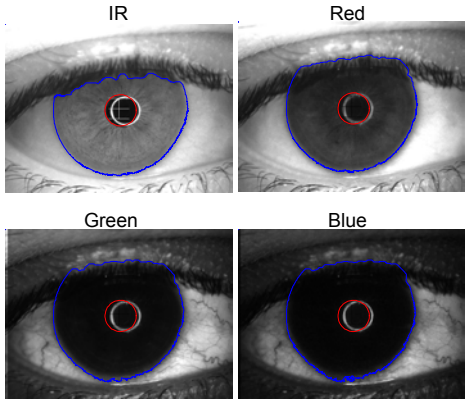

Figure 8. Result of segmentation on the IR, red, green, and blue channels of a brown iris image.

6. Feature Extraction and Matching

After segmentation, the extracted iris was unwrapped and converted to the polar domain (see [1]). Thus, the iris was processed as a rectangular entity rather than a circular one. A modified version of Daugman's algorithm was used to extract textural information from the unwrapped iris. Feature extraction is accomplished by subjecting the rectangular iris to a set of three Gabor filters and observing the phase-response of the filtered image. All three filters had the same orientation and frequency but represented different scales. Each Gabor filter was applied to a different region in the rectangular image since the level of iris detail typically degrades as one moves away from the pupil. The feature set pertaining to a segmented iris consisted of an array of binary values and, thus, the hamming distance was used to compare two such feature sets. In the future, a different algorithm will be used to elicit and represent the rich textural content of the iris as revealed in the multispectral image.

7. CIE L*a*b* Histogram Equalization

Adaptive histogram equalization was performed in the CIE L*a*b* color space to enhance the structural components across the various spectral channels of the iris image. In the L*a*b* space, the intensity values are represented by the L* parameter, the colors between green and magenta are represented by the a* parameter and the colors between blue and yellow by the b* parameter. Thus, histogram equalization can be performed on the L* component without affecting the original color of the image. This color space was used in our experiments since the goal was to moderate the intensity values without perturbing the color components. The effect of this transformation, and the subsequent equalization, is the retention of the original color information, with certain iris components being emphasized in the individual spectral channels.

In order to facilitate transformation from the original color space to L*a*b*, the following two mappings were examined: (a) the IR-R-G (false color or CIR) information was converted to the L*a*b* space; and (b) the R-G-B information was converted to the L*a*b* space. In both these cases, after histogram equalization, the information was converted back to the CIR/RGB space. The result of histogram equalization based on these two mappings can be seen in Figure 7.

To study the importance of this mapping and equalization, the following experiment was conducted. Iris matching was performed on the individual spectral channels before and after the aforementioned equalization scheme. The ROC (Receiver Operating Characteristic) curves in Figure 8 indicate the substantial improvement in performance associated with the blue channel. This may be attributed to the exchange of pertinent information (related to image contrast) across multiple channels during the equalization process.

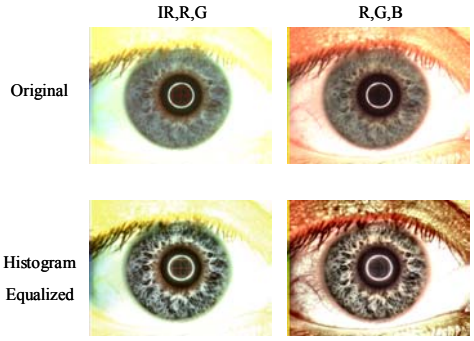

Figure 7. The CIR (IR-R-G) and RGB color images before (top) and after (bottom) L*a*b* color space image adaptive histogram equalization.

8. Cross Channel (Wavelength) Matching

The possibility of matching iris images across multiple wavelengths was next studied. Thus, the following comparisons were performed: IR vs. R, IR vs. G, IR vs. B, R vs. G, R vs. B, and G vs. B.

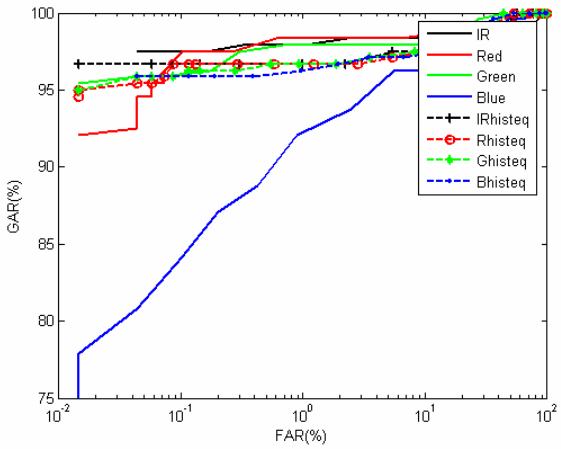

Figure 8. The effect of L*a*b* histogram equalization on matching performance. The blue channel is observed to result in improved performance as a result of this equalization.

Figure 9 suggests that the cross matching performance decreases as a function of the differences in wavelength of the participating images. For example, the IR (850nm) and the Blue (475nm) channels are separated by the greatest range across the electromagnetic spectrum. Therefore, the reflective texture response varies the greatest across this range. When matching images in these two ranges, significant variations in texture response results in inferior

performance. This can be seen across the other spectral ranges as well. On the other hand, spectral channels whose differences in wavelength are relatively small do not exhibit such a drastic decrease in matching performance. For example, the ROC curve corresponding to G vs. B is observed to be better than that corresponding to IR vs. B. This phenomenon indicates that different wavelengths highlight various textural components of the iris, further underscoring the importance of conducting multispectral iris analysis.

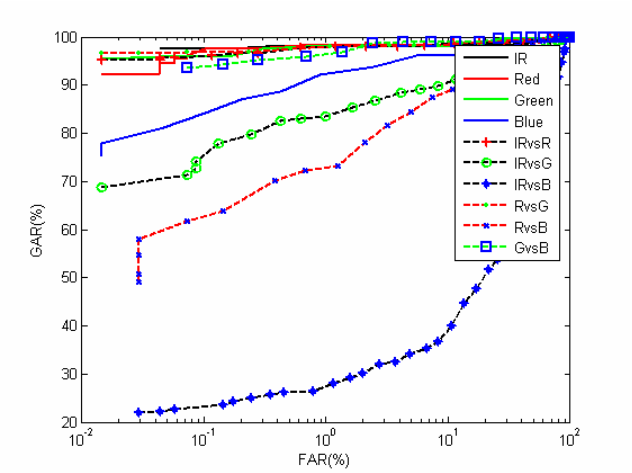

Figure 9. ROC curves indicating the cross channel matching performance.

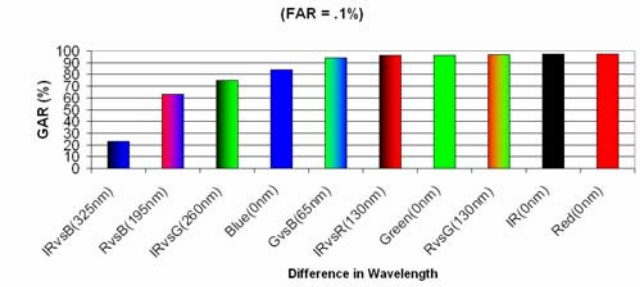

Figure 10. Plotting the Genuine Accept Rate (GAR) as a function of difference in wavelengths of participating images.

9. Iris Component Clustering

The goal of the multispectral clustering analysis presented in this section is to determine if there are any structural components of the iris (e.g., crypts, stroma, furrows, moles, freckles) that can be consistently categorized across irides of different colors. The other advantage of such an analysis is the ability to segment the iris itself from the sclera and the eye lashes. Indeed, as previously stated, the segmentation algorithm can be suitably modified to use information across the spectral channels in order to enhance the segmentation process. Thus, an inaccurately segmented image (or more specifically, an over-segmented image) can be more accurately segmented by employing the clustering procedure described below. Research in this direction could potentially lead to new and more efficient iris segmentation algorithms.

To reduce the computational complexity of processing, the image pixels were first averaged with a 4x4 smoothing filter and then down-sampled (within individual spectral channels). Each pixel in this new image was then viewed as a three dimensional vector, with each value in this vector corresponding to the intensity of the R, G or B channels. The K-means clustering algorithm was used to categorize the pixels based on these 3-dimensional vectors. The Euclidean distance metric was employed to determine the 'distance' between two pixels. It was observed that for blue-colored irides, the different components of the iris were separated into multiple clusters (Figure 11). However, more experiments need to be conducted in order to determine if component decomposition is feasible for all eye colors. This would entail the application of appropriate image normalization schemes and adoption of alternate distance metrics to better compare pixels.

The clustering procedure was next repeated for iris images that were intentionally over-segmented by 100 pixels radially into the sclera. Clustering results for the over-segmented images indicate the successful segmentation of the sclera, eyelashes and iris into separate components as seen in Figure 12. This clustering experiment was also conducted by viewing each pixel as an IR-R-G-B entity (4-dimensional vector) and as an L*a*b* entity (3-dimensional vector). The results of these clustering procedures can be seen in Figure 13 and Figure 14, respectively.

10. Fusion of Multispectral Information

In the final experiment, the sum rule was used to fuse the match scores generated for each spectral channel (Figure 15). Combining the blue channel with any of the other channel results in a substantial improvement in performance. However, it must be noted that our small database contained a preponderance of brown irides. Therefore, the matching performance using the blue channel (only) is lower than the other three channels. More sophisticated fusion schemes (at the image/feature level) may be necessary to exploit the complementary information presented by the multiple channels. In general, the IR and Red channels are observed to perform very well for the brown irides. We anticipate that for irides of other colors, the use of multispectral information will be beneficial.

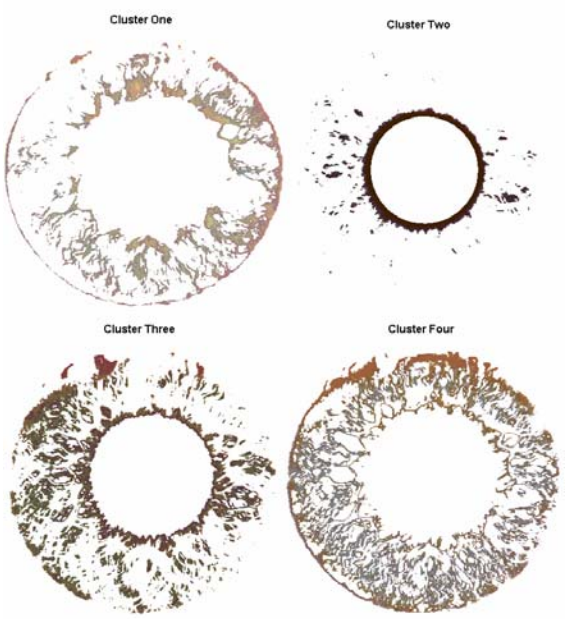

Figure 11. Individual clusters of a blue iris that was subjected to K-means clustering in the RGB domain (K=4). The iris is assumed to be properly segmented.

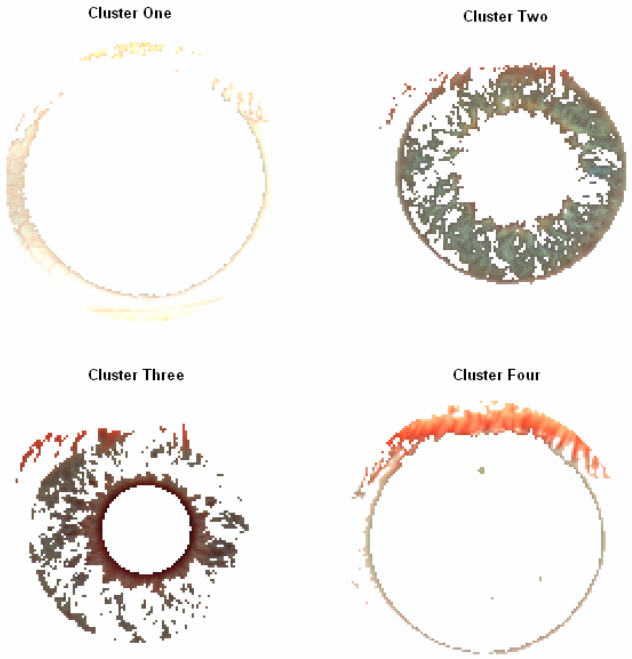

Figure 13. Results of clustering pixels in the IR-R-G-B domain (K=4) on an iris image that was deliberately over-segmented. In this example, clusters 1 and 4 appear to extract pixels corresponding to the eye-lashes and skin.

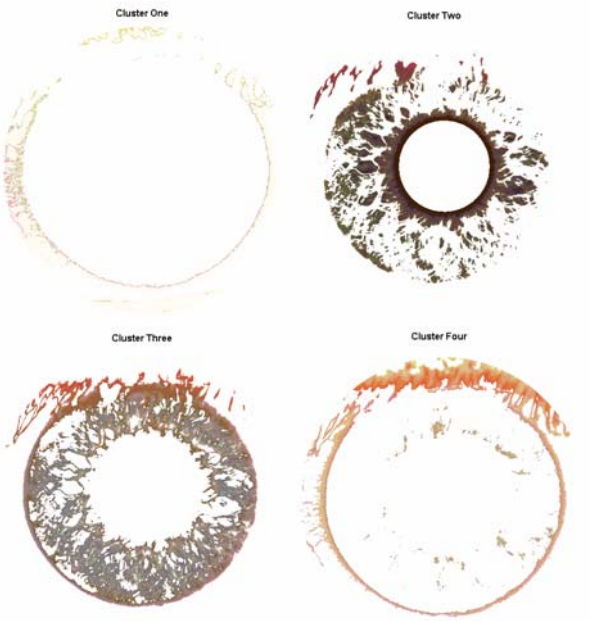

Figure 12. Individual clusters of a blue iris which has been over segmented by a value of 100 pixels into the sclera radially. It is observed that some of the clusters contain the eyelash information.

Figure 14. Results of clustering pixels in the L*a*b* domain (K=4) on an over-segmented iris image. Here, clusters 1 and 2 appear to isolate the non-iris portions of the image.

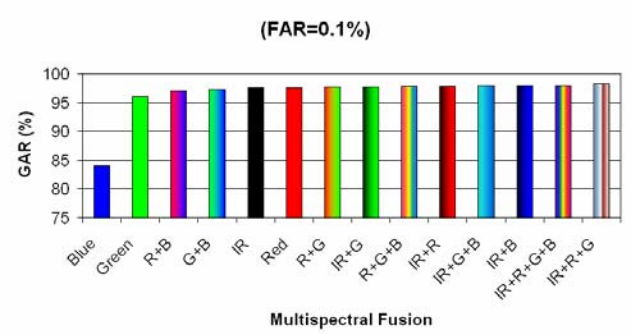

Figure 15. Score level fusion of multispectral information. The genuine accept rate (GAR) has been reported at a FAR of 0.1% In this case, no histogram equalization was performed on the individual channels.

11. Summary and Future Work

The purpose of this paper was to highlight the potential of using multispectral iris information in recognition systems. Since most commercial systems use only the near-IR wavelengths for iris analysis, there is lack of literature discussing the benefits of employing multispectral information that includes the visible portion of the electromagnetic spectrum. Depending upon the color of the eye, the nature of iris information presented in different spectral channels can vary. This presents the novel possibility of utilizing user-specific wavelengths for iris image acquisition. Furthermore, the use of multispectral information has the potential to enhance the segmentation and enhancement procedures thereby improving the performance of iris recognition systems. Pixel-clustering based on color information may be used to elicit and examine the various components of the iris. One application of such an analysis would be the detection of moles and freckles present on the surface of the iris. The analysis of multispectral images also provides the option of processing the iris information contained in high resolution color images of the face.

References

[1] J. Daugman, "High confidence visual recognition of persons by a test of statistical independence," IEEE Transactions on Pattern Analysis and Machine Intelligence, Vol. 15, No. 11, pp. 1148-1161, 1993.

[2] L. Masek, "Recognition of Human Iris Patterns for Biometric Identification," BSE Dissertation, University of Western Australia, 2003.

[3] L. Ma, T. Tan, Y. Wang, D. Zhang, "Efficient Iris Recognition by Characterizing Key Local Variations," IEEE Transactions on Image Processing. Vol. 13, No. 6, June 2004.

[4] D. Socolinsky, L. Wolff, "A New Paradigm for Multispectral Imagery and Data Fusion," IEEE Computer Society Conference on Computer Vision and Pattern Recognition (CVPR'99), Vol. 1, pp. 319-324, Ft. Collins, CO, 1999

[5] Z. Pan, G. Healey, M. Prasad, B. Tromberg, "Face Recognition in Hyperspectral Images," IEEE Transactions on Pattern Analysis and Machine Intelligence, Vol. 25, No. 12, Dec. 2003.

[6] B. Abidi, S. Huq, M Abidi, "Fusion of Visual, Thermal, and Range as a Solution to Illumination and Pose Restrictions in Face Recognition." IEEE Carnahan Conf. Security Technology, pp. 325-330, Albuquerque, NM, October 2004.

[7] R. Rowe, K. Nixon, S. Corcoran, "Multispectral Fingerprint Biometrics," Proceedings of the IEEE Workshop on Information Assurance and Security, West Point, NY, 2005.

[8] T. Sakamoto, C. Nakanishi, T. Hase, "Software Pixel Interpolation for Digital Still Cameras Suitable for a 32-Bit MCU." IEEE Transactions on Consumer Electronics, Vol. 44, No. 4, pp. 1342-1352, November 1998.

[9] S. Fan, C. Dyer, L. Hubbard, "Quantification and Correction of Iris Color," Technical Report 1495, University of Wisconsin-Madison, 2003

[10] A. Wielgus, T. Sama, "Melanin In Human Irides Of Different Color And Age Of Donors." Pigment Cell Res., Vol. 18, No. 6, pp. 454-464, December 2005.

[11] A. Wielgus, T. Sarna, "Photogeneration of Superoxide Anion by Iris of the Human Eye Under *in vitro* Conditions." Current Topics in Biophysics, Vol. 26, No. 1, pp. 163-174, 2002.

[12] R. Snell, M. Lemp. *Clinical Anatomy of the Eye*. Blackwell Science, 1998.